International Journal of Mechatronics, Electrical and Computer Technology

Vol. 4(12), Jul, 2014, pp. 857-885, **ISSN**: 2305-0543
Available online at: http://www.aeuso.org

Active and Reactive Power Control of Photovoltaic Systems Connected to the Network for Maximum Power Point Tracking

Meysam Amoozadeh and S. Asghar Gholamian

Babol University of Technology,

Faculty of Electrical and Computer Engineering, Babol, Iran

*Corresponding Author's E-mail: *gholamian@nit.ac.ir*

Abstract

This paper proposes an intelligent control technique using a fuzzy logic controller (FLC) to obtain the maximum available power of PV module under unstable conditions. Control of the presented system is based on instantaneous power theory (p-q theory) and adaptive hysteresis band control (AHBC). According to this strategy during sunlight the system sends active power to the grid and at the same time compensates the reactive power of the load. In case there is no sunlight the inverter only compensates the reactive power of the load. Variable switching frequency due to fixed hysteresis bands known as a drawback of hysteresis method used in power system applications. To solve this problem, adaptive hysteresis current control (AHCC) has been introduced. Simulation results using MATLAB/SIMULINK verifies effectiveness of the system in injecting of maximum power and compensating of the harmonic currents and reactive power of the nonlinear load.

Keywords: Photovoltaic, MPPT, Fuzzy, Adaptive hysteresis band

1. Introduction

Recently, renewable-energy resources have been becoming popular due to the decrease of fuel sources, their negative effects of global warming and damages to the environment. Solar energy is one of these alternative energy resources. It is converted to the electrical energy by photovoltaic (PV) arrays. PV arrays do not generate any toxic or harmful substances that

Vol. 4(12), Jul, 2014, pp. 857-885, ISSN: 2305-0543
Available online at: http://www.aeuso.org

pollute the environment another considerable feature of them are the requirement of low maintenance. Therefore, studies on PV systems have increased gradually [1]. On the other hand, during the exploitation of the conventional electric power network, the quality problem of the electric power energy provided to the users has arisen. This is due to the increasing presence on the network of nonlinear loads; they constitute a harmonic pollution source of to the network, which generate many disturbances, and disturb the optimal operation of electrical equipments [2]. Active and passive filters are investigated for this purpose. Passive filter is capacitors to the renounced problem with grid. Active power filters in which inverter and semiconductor device is required don't have the resonance problem of passive filters; these filters are smaller and lighter than passive ones; hence using of these filters have been rapidly increased [3]. The sunlight intensity is time variant and sometimes changes rapidly in a day, because of this, the optimum operation point of PV module moves from one curve to another. So the maximum power point tracker must track the maximum point rapidly possible in order to alleviate the oscillation of output power of PV module [4]. Among the proposed methods, intelligent control is surrogated the conventional algorithms like P&O, INC and so on [5-6]. Fuzzy logic control is an intelligent method which has simplicity and effectiveness in linear and nonlinear systems. In addition, this control has high implication in maximum power point tracking in photovoltaic systems [7]. For example, the ref. [8] corroborated that the FLC reach to maximum power point eight times better than conventional P&O algorithm. In this paper, intelligent control method using the fuzzy logic controller is proposed to obtain better performance of energy conversion. PV module produces electricity in DC voltage for grid integrated system or supplying a standalone AC load, the DC voltage should be converted to the AC voltage using DC/AC inverters. By proper switching of these inverters, the system not only injects active power of the PV into the grid, but also can eliminate or mitigate harmonics of nonlinear loads [9]. The effectiveness of active power filter depends upon the design and characteristics of the current controller. There is various PWM current control strategies proposed for APF applications [10]. In this paper, an adaptive hysteresis

International Journal of Mechatronics, Electrical and Computer Technology

Vol. 4(12), Jul, 2014, pp. 857-885, **ISSN**: 2305-0543
Available online at: http://www.aeuso.org

band control method is introduced and used for injecting the proper current into the grid. Using this method will solve the problem of frequency changing in the conventional fix band hysteresis controller [11]. Figure1 shows the proposed system; three wire systems and nonlinear loads. Reference current is generated using p-q theory. The actual current of the PV-AF system and the reference current are compared to generate switching pulses of the inverter switches according to the adaptive hysteresis band.

2. PV cell model and electric characteristics

Accurate mathematical model is necessary to represent the electric characteristics of PV module [12]. The conventional equivalent circuit of solar cell is expressed by one or two diode whereas representing by a photo current source, parallel diode, shunt resistance (R_{sh}) and series resistance (R_s) as seen in Figure 2. The current source (I_{ph}) models the sunlight energy conversion, the shunt resistance represents the consequence of leaks, the series resistant represents the various resistances of connections and the diodes model the PN junctions [13].

The photocurrent generated by the PV module is given by equations 1 and 2:

$$I = I_{ph} - I_{d1} - I_{d2} - I_{RP} \tag{1}$$

$$I = I_{ph} - I_{S1} \times (\exp \frac{q.(V + R_S.I)}{A_1.k.T} - 1) - I_{S2} \times (\exp \frac{q.(V + R_S.I)}{A_2.k.T} - 1) - \frac{V + R_S.I}{R_{Sh}} \tag{2}$$

Where V and I is the PV module voltage and current; $A_{1,2}$ is ideality factor of PV junctions; $I_{s1,2}$ is saturation current of diodes; q is the electronic charge; K is Boltzmann's constant and T the cell temperature. Table (1) lists parameters of the simulated PV module.

International Journal of Mechatronics, Electrical and Computer Technology

Vol. 4(12), Jul, 2014, pp. 857-885, **ISSN**: 2305-0543

Available online at: http://www.aeuso.org

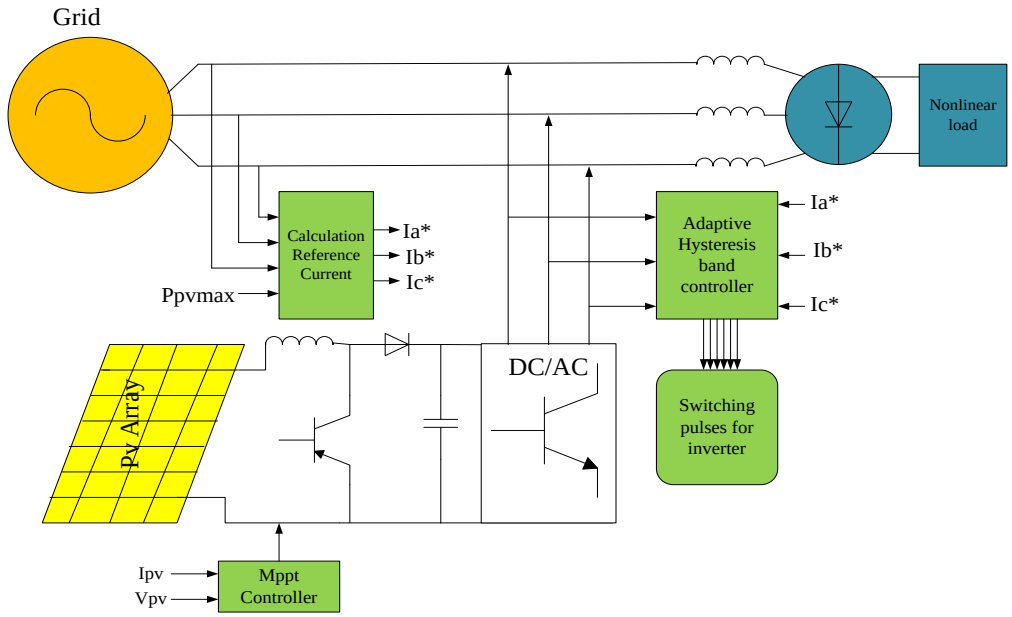

Figure1. This proposed configuration

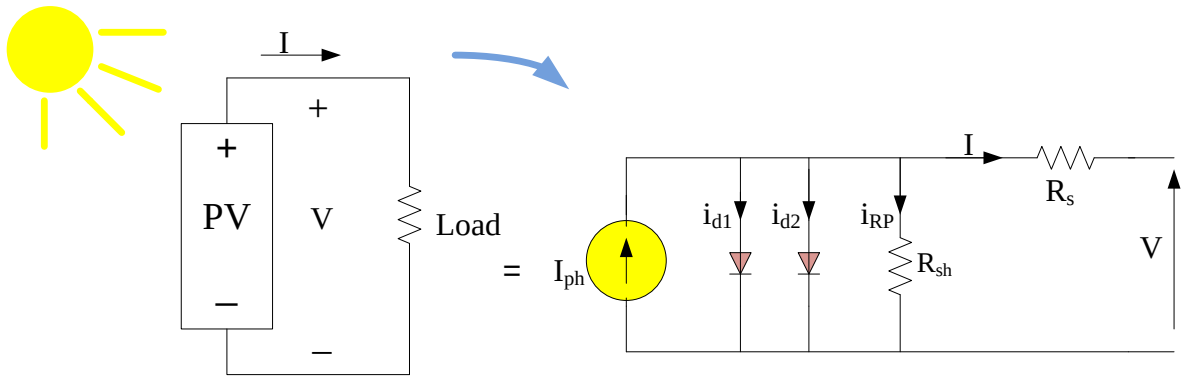

Figure 2. Equivalent circuit of PV cell [14]

International Journal of Mechatronics, Electrical and Computer Technology

Vol. 4(12), Jul, 2014, pp. 857-885, **ISSN**: 2305-0543
Available online at: http://www.aeuso.org

Table1. BP SX 150S data sheet [15]

Model	BP SX 150S
Maximum power (Pmax)	150W
Voltage at Pmax (Vmp)	34.5V
Current at Pmax (Imp)	4.35A
Short-circuit current (Isc)	4.75A
Open-circuit voltage (Voc)	43.5V
Temperature coefficient of Isc	(0.065±0.015)%/°C
Temperature coefficient of Voc	-(160±20)mV/°C
Temperature coefficient of power	-(0.5±0.05)%/°C
NOCT	47±2°C
Number of parallel PV modules	6
Number of PV modules in series	6
Reference temperature	$25^{\circ c}$
Reference solar radiation	$1000W/m^2$

The P-V curve of this PV array under G=1 kw/m^2 , T=25 ^oC and G=0.75 kw/m^2 , T=23^oC and G=0.5 kw/m^2,T=18 ^oC solar irradiance and temperature is shown in Figure3

International Journal of Mechatronics, Electrical and Computer Technology

Vol. 4(12), Jul, 2014, pp. 857-885, **ISSN**: 2305-0543
Available online at: http://www.aeuso.org

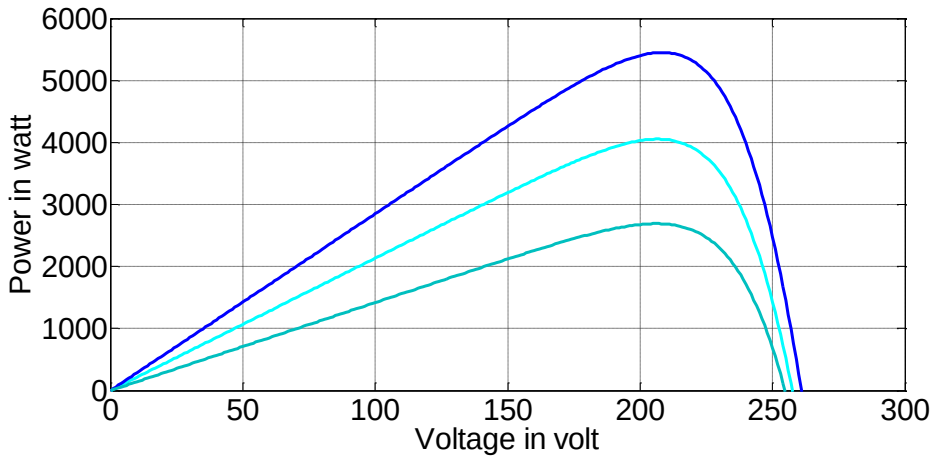

Figure 3. P-V characteristic of the PV array

The output power of PV module is dependent on two parameters, sunlight intensity and PV cell temperature. Solar irradiance has direct relation and temperature has reverse relation with output power of PV module. It means increasing the sunlight intensity; the output power rises up. Increasing the temperature; the power comes down. Figure 4 and Figure 5 show the output characteristics of PV module under variable sunlight intensity and different temperatures.

International Journal of Mechatronics, Electrical and Computer Technology

Vol. 4(12), Jul, 2014, pp. 857-885, **ISSN**: 2305-0543

Available online at: http://www.aeuso.org

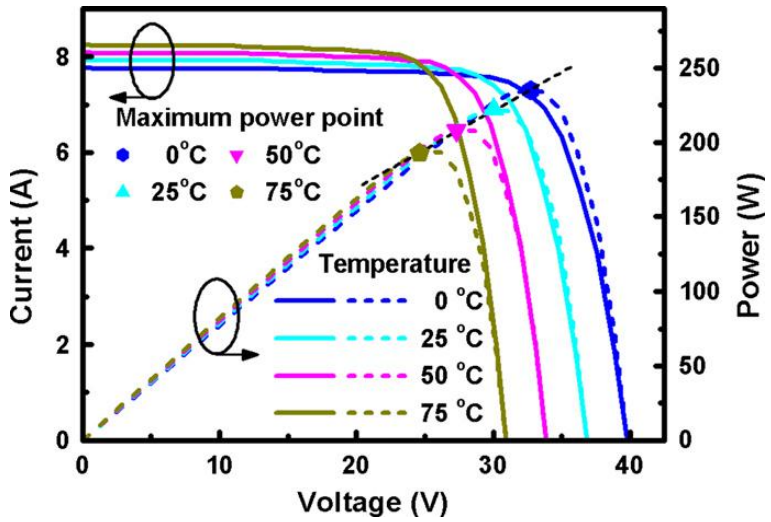

Figure4. I-V and P-V characteristics of a PV module for different temperature[16]

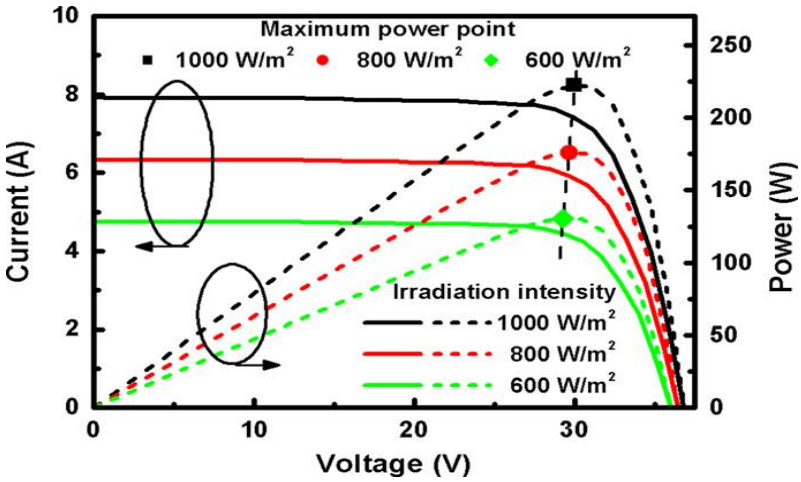

Figure5. I-V and P-V characteristics of a PV module for varied sunlight intensity [16]

International Journal of Mechatronics, Electrical and Computer Technology

Vol. 4(12), Jul, 2014, pp. 857-885, ISSN: 2305-0543
Available online at: http://www.aeuso.org

3. MPPT Technique and Fuzzy Logic Controller

There are several MPPT techniques as hill-climbing, P&O, Incremental Conductance. These are conventional methods and have some drawbacks such as [17]:

- Converging to maximum operation point is slow.
- Oscillation of PV power amplitude around MPP is considerable that cause power losses.
- When the irradiance changes quickly, the system response is slow and moves away from MPP.

To conquer these drawbacks, modern MPPT techniques such as Fuzzy Logic Controller, neural network and intelligent method are proposed [18, 19].

Fuzzy logic controller properly performs in nonlinear systems. It is on the basis of designer knowledge rather than accurate mathematical model. FLC consists of four categories as fuzzification, inference engine, rule base and defuzzification. In the first section, numerical input variable are converted into fuzzy variable known as linguistic variable [20]. Inference engine defines controller output in order to fuzzify input, rule base and fuzzy inference methods. Rule base section consists of "if A and B and C then D" forms. Finally output linguistic terms are converted to numerical variable in defuzzification section. Figure 6 shows the fuzzy inference system. Equations (3 - 5) express the inputs of FLC; E, CE and V_{pv}. The defuzzification uses center of gravity to compute the output of FLC (ΔD) as equation (6).

$$INPUT1: E(t) = \frac{P_{pv}(t) - P_{pv}(t-1)}{V_{pv}(t) - V_{pv}(t-1)} \tag{3}$$

$$INPUT2: CE(t) = E(t) - E(t-1) \tag{4}$$

International Journal of Mechatronics, Electrical and Computer Technology

Vol. 4(12), Jul, 2014, pp. 857-885, **ISSN**: 2305-0543
Available online at: http://www.aeuso.org

$$INPUT3: V(t) \tag{5}$$

$$\Delta D = -\frac{\sum_{j=1}^{n} \bar{y} D_j}{\sum_{j=1}^{n} D_j} \tag{6}$$

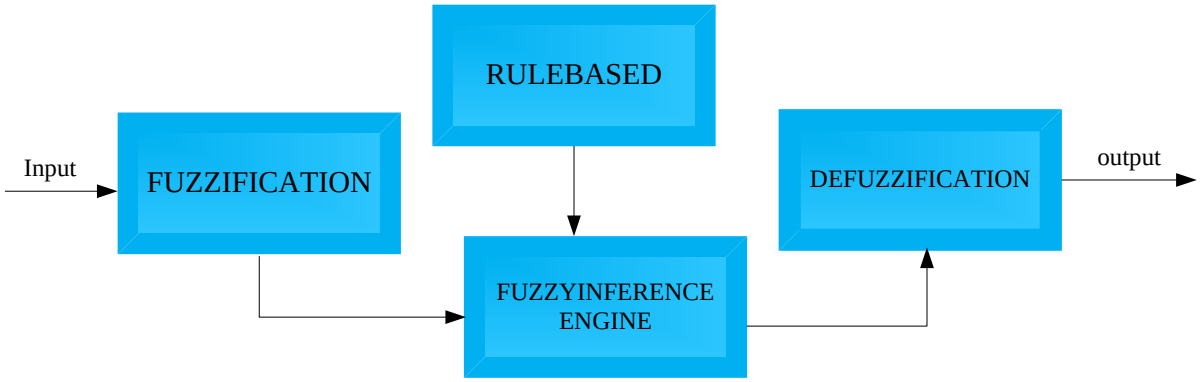

Figure6. Fuzzy inference system [21]

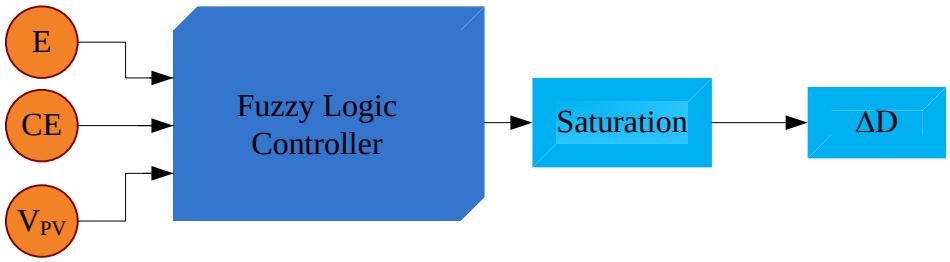

Figure7. Configuration of MPPT algorithm with Fuzzy Logic Controller

International Journal of Mechatronics, Electrical and Computer Technology

Vol. 4(12), Jul, 2014, pp. 857-885, **ISSN**: 2305-0543
Available online at: http://www.aeuso.org

Figure 8 shows fuzzy membership functions for E, CE, Vpv and ΔD. The terms N,Z,P,L and G respectively mean negative, zero, positive, little and great. The output membership functions are nominated as mf1 to mf9. The extent of membership functions parameter are {-10, 10}, {-10, 10}, {205, 215} for inputs and {-1, 1} for the output. The fuzzy inference is carried out by mamdani's method. The control rules are indicated in Table 2.

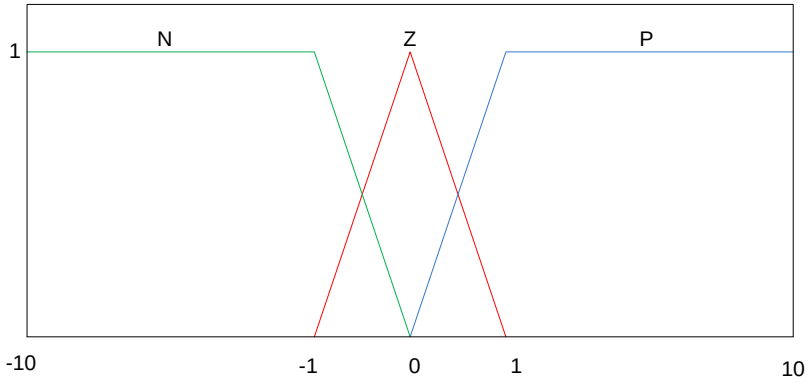

(8-a)

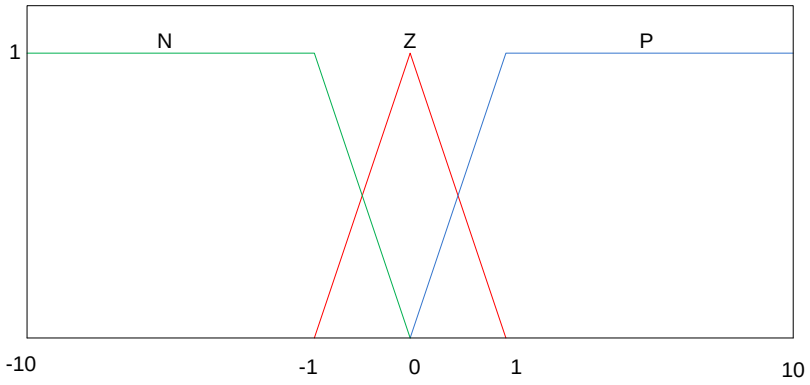

(8-b)

International Journal of Mechatronics, Electrical and Computer Technology

Vol. 4(12), Jul, 2014, pp. 857-885, **ISSN**: 2305-0543
Available online at: http://www.aeuso.org

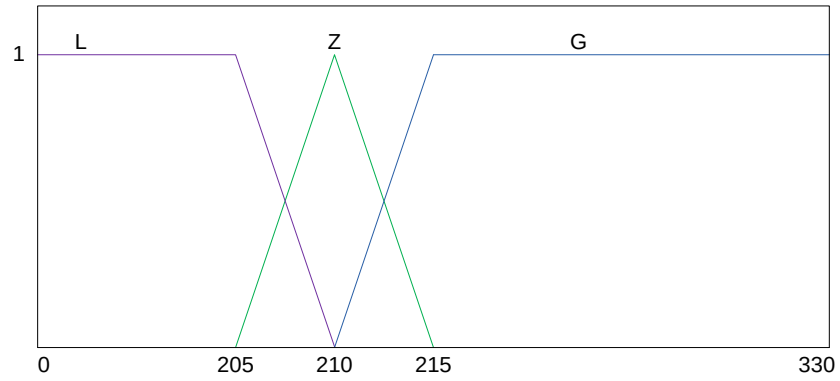

(8-c)

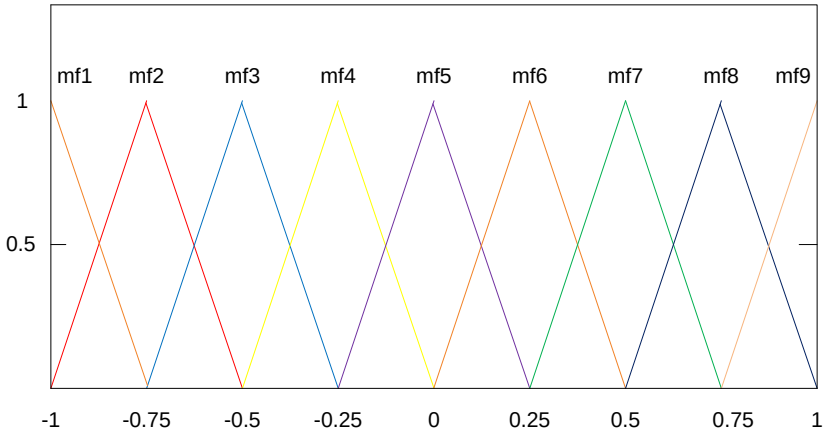

(8-d)

Figure8. Membership functions, a) first input, b) second input, c) third input, d) output

The FLC reduce the output power oscillations of photovoltaic module. The simulated circuit is shown in Figure.9. To verify of the simulation, the solar irradiance is changed from G= 1 kw/m^2 and T=25 ^{o}C to G=0.75 kw/m^2 and T=23 ^{o}C at t=0.5s. The output power of the PV array is shown in Figure.10. This figure shows that delivered power is about 5400 watt under

International Journal of Mechatronics, Electrical and Computer Technology

Vol. 4(12), Jul, 2014, pp. 857-885, **ISSN**: 2305-0543
Available online at: http://www.aeuso.org

G=1 kw/m^2 and T=25^{o}C By decreasing the irradiance to G=0.75 kw/m^2 and T=23 ^{o}C, the output power of the PV changes to about 4030 watt.

Table2. Fuzzy rules

input1	input2	input3	output
N	N	Z	Mf4
N	N	G	Mf1
N	Z	Z	Mf3
N	Z	G	Mf1
N	P	Z	Mf5
N	P	G	Mf4
Z	N	Z	Mf4
Z	N	G	Mf2
Z	Z	Z	Mf5
Z	P	L	Mf8
Z	P	Z	Mf6
Z	P	G	Mf4
P	N	L	Mf7
P	N	Z	Mf5
P	Z	L	Mf7
P	Z	Z	Mf6
P	P	L	Mf9
P	P	Z	Mf7

International Journal of Mechatronics, Electrical and Computer Technology

Vol. 4(12), Jul, 2014, pp. 857-885, **ISSN**: 2305-0543
Available online at: http://www.aeuso.org

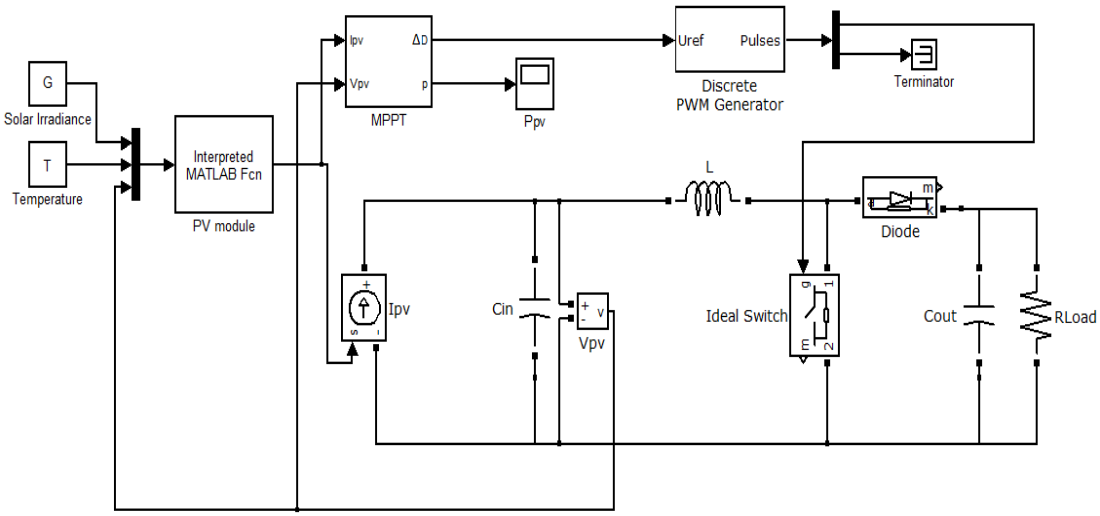

Figure9. PV and MPPT configuration

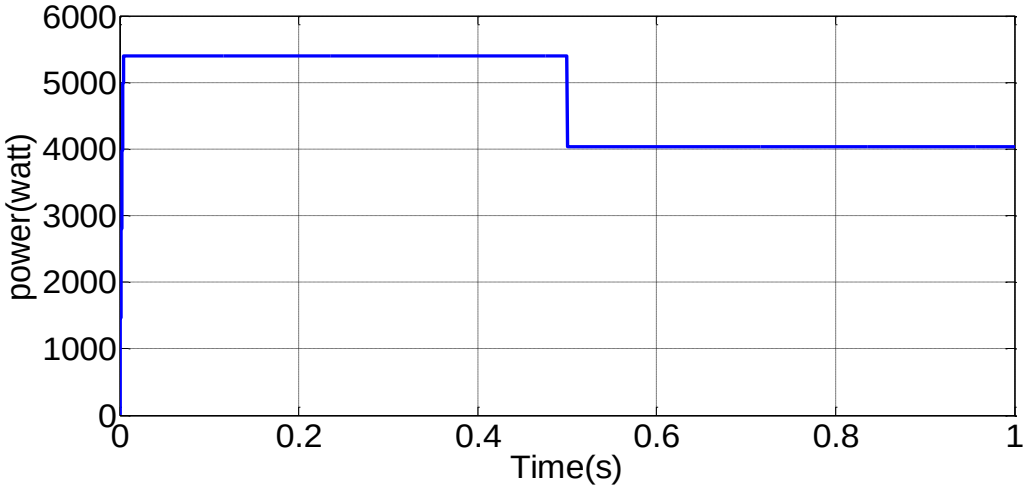

Figure10. Output power of the PV system

International Journal of Mechatronics, Electrical and Computer Technology

Vol. 4(12), Jul, 2014, pp. 857-885, **ISSN**: 2305-0543
Available online at: http://www.aeuso.org

4. Active and reactive power

Generating proper reference current signal is important to inject maximum power of PV into the grid and compensating reactive and active current of nonlinear load. As mentioned before, p-q theory can generate this reference current [22]. In this method, a set of voltages (va, vb, vc) and currents (ia, ib, ic) from phase coordinates are first transferred to the α-β coordinates using Clark's transformation [23].

$$\begin{bmatrix} v\alpha \\ v\beta \end{bmatrix} = \begin{bmatrix} 1 & -1/2 & -1/2 \\ 0 & \sqrt{3}/2 & -\sqrt{3}/2 \end{bmatrix} \cdot \begin{bmatrix} v_a \\ v_b \\ v_c \end{bmatrix} \tag{7}$$

$$\begin{bmatrix} i\alpha \\ i\beta \end{bmatrix} = \begin{bmatrix} 1 & -1/2 & -1/2 \\ 0 & \sqrt{3}/2 & -\sqrt{3}/2 \end{bmatrix} \cdot \begin{bmatrix} ia \\ ib \\ ic \end{bmatrix} \tag{8}$$

The instantaneous power for the three-phase system is as follows:

$$\begin{bmatrix} p \\ q \end{bmatrix} = \begin{bmatrix} v\alpha & v\beta \\ -v\beta & v\alpha \end{bmatrix} \cdot \begin{bmatrix} i\alpha \\ i\beta \end{bmatrix} \tag{9}$$

Where p is the instantaneous real power .q is the instantaneous imaginary power. By observing the formulations of p and q , it is possible to put them in the following form:

$$\begin{aligned} p &= \bar{p} + \tilde{p} \\ q &= \bar{q} + \tilde{q} \end{aligned} \tag{10}$$

$\bar{p}$ in watts is the DC term of the instantaneous real power and represents the conventional active power injected from the source into the load in the positive sequence. $\tilde{p}$ in energy per

International Journal of Mechatronics, Electrical and Computer Technology

Vol. 4(12), Jul, 2014, pp. 857-885, **ISSN**: 2305-0543
Available online at: http://www.aeuso.org

time, is the oscillation part of the real instantaneous power represent the exchanged power between the source and load in the a-b-c coordination system.

q¯ is the DC part of the imaginary power represents the conventional reactive power and q˜ is the oscillation part of the imaginary power represents the power exchanged between different phases of a three phase system [24].The PV-AF system should compensate the reactive power and the oscillation part of the real and imaginary part of the source current; furthermore the reference current should be able to inject maximum power of the PV (Ppvmax) into the grid. Hence the system should inject –(Ppvmax+ p˜) as the real power and -q as the imaginary power. The reference current in α-β is given by (11):

$$\begin{bmatrix} i\alpha \\ i\beta \end{bmatrix} = \begin{bmatrix} v\alpha & v\beta \\ -v\beta & v\alpha \end{bmatrix}^{-1} \begin{bmatrix} -p_{\max\, pv} - p \\ -q \end{bmatrix} \tag{11}$$

The reference current in the a-b-c coordination is calculated by (12):

$$\begin{bmatrix} ia^{*} \\ ib^{*} \\ ic^{*} \end{bmatrix} = \sqrt{\frac{2}{3}} \begin{bmatrix} 1 & 0 \\ -1/2 & \sqrt{3}/2 \\ -1/2 & -\sqrt{3}/2 \end{bmatrix} \begin{bmatrix} i\alpha \\ i\beta \end{bmatrix} \tag{12}$$

5. Adaptive hysteresis band control

The hysteresis band current control technique has proven to be most suitable for all the applications of current controlled voltage source inverters. The hysteresis band current control is characterized by unconditioned stability, very fast response, and good accuracy. On the other hand, the basic hysteresis technique exhibits also several undesirable features; such as uneven switching frequency that causes acoustic noise and difficulty in designing input

International Journal of Mechatronics, Electrical and Computer Technology

Vol. 4(12), Jul, 2014, pp. 857-885, **ISSN**: 2305-0543
Available online at: http://www.aeuso.org

filters [25]. In the conventional hysteresis band controller as shown in Figure.11, the reference current Ia* is compared with actual current Ia and switching pulses are generated according to the following logical function. If (Ia – Ia*> HB) , in other word, if the current reach to its upper limit, the upper switch become off (S4=1, S1=0) . If (Ia – Ia*<-HB), in other word, if the current reach to its lower limit the upper switch become on (S4=0, S1=1). This function is the same for phase b and c except phase shifts. As mentioned before, in this algorithm switching frequency is depended on the rate of actual current delivered by the inverter.

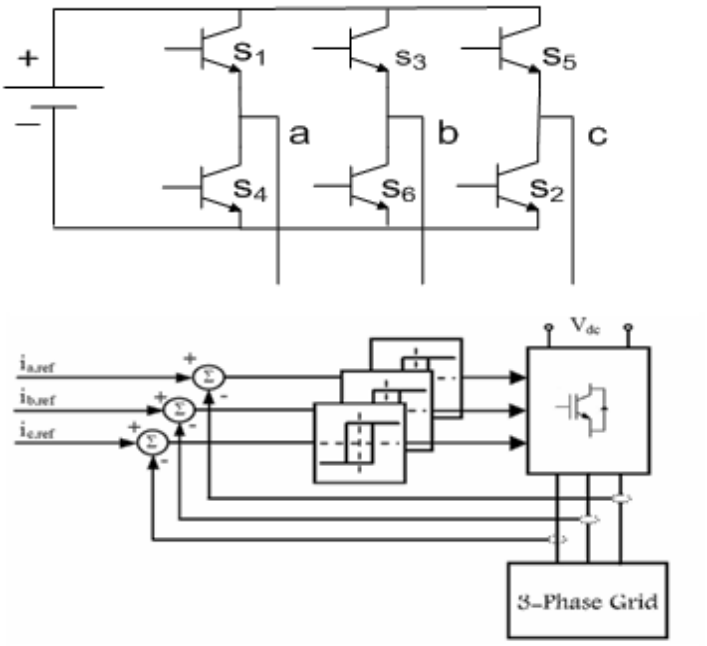

Figure11. Hysteresis band control

In active filter application, inductance of the filter and DC link voltage determine the current rate. In the conventional hysteresis band algorithm, the band width is kept constant. By

International Journal of Mechatronics, Electrical and Computer Technology

Vol. 4(12), Jul, 2014, pp. 857-885, **ISSN**: 2305-0543
Available online at: http://www.aeuso.org

changing the hysteresis bandwidth which determines the shape of the error, the average frequency will be controlled. In the active power filter application, high frequency causes better harmonic compensation. It is restricted by the EMI and switching loss problems [24]. Figure.12 shows the PWM current and voltage waveforms for phase a. When the currents ia tend to cross the lower hysteresis band at point 1, where S1 is switched on. The linearly rising current (ia^+) then touches the upper band at point P, where is S4 switched on. The following equations can be written in the respective switching intervals t_1 and t_2 from Figure.12. [25]

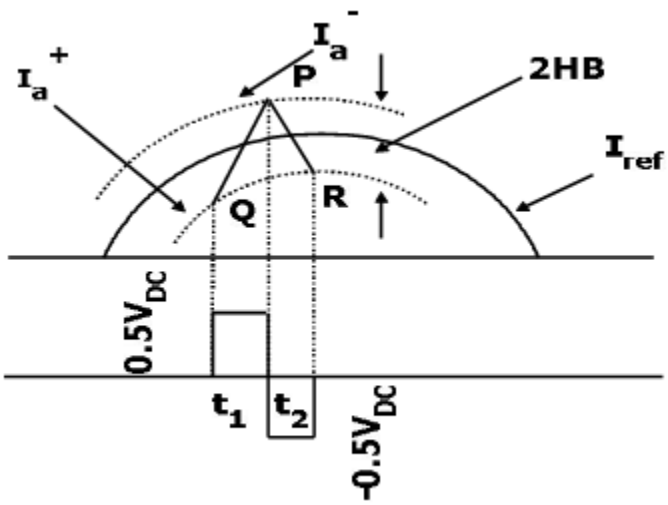

Figure12. Current and voltage wave with hysteresis band current control

For the respective switching intervals of t_1 and t_2 we will have:

$$\frac{dia^+}{dt} = \frac{1}{L}(0.5Vdc - Va) \tag{13}$$

International Journal of Mechatronics, Electrical and Computer Technology

Vol. 4(12), Jul, 2014, pp. 857-885, **ISSN**: 2305-0543
Available online at: http://www.aeuso.org

$$\frac{dia^{-}}{dt} = -\frac{1}{L}(0.5Vdc + Va) \tag{14}$$

As shown in Figure12 it can be written:

$$\frac{dia^{+}}{dt}t_1 - \frac{dia^{*}}{dt}t_1 = 2HB \tag{15}$$

$$\frac{dia^{-}}{dt}t_2 - \frac{dia^{*}}{dt}t_2 = -2HB \tag{16}$$

$$t_1 + t_2 = T_c = \frac{1}{f_c} \tag{17}$$

Adding Equ.15 and Equ.16 and substituting it to Equ.17 gives us the follows:

$$\frac{dia^{+}}{dt}t_1 + \frac{dia^{-}}{dt}t_2 - \frac{1}{f_c}\frac{dia^{*}}{dt} = 0 \tag{18}$$

Subtracting Equ.16 from Equ15, it can be written:

$$\frac{dia^{+}}{dt}t_1 - \frac{dia^{-}}{dt}t_2 - (t_1 - t_2)\frac{dia^{*}}{dt} = 4HB \tag{19}$$

Substituting Equ.14 to Equ.19, we can get:

$$(t_1 + t_2)\frac{dia^{+}}{dt} - (t_1 - t_2)\frac{dia^{*}}{dt} = 4HB \tag{20}$$

Substituting Equ.14 to Equ.18 and simplifying it we will have:

International Journal of Mechatronics, Electrical and Computer Technology

Vol. 4(12), Jul, 2014, pp. 857-885, **ISSN**: 2305-0543
Available online at: http://www.aeuso.org

$$t_1 - t_2 = \frac{\frac{dia^*}{dt}}{f_c(\frac{dia^+}{dt})} \tag{21}$$

Substituting Equ.21 to Equ.20, it can be written:

$$HB = \frac{Vdc}{8 f_c L}[1 - \frac{4L^2}{Vdc^2}(\frac{V_a}{L} + m)^2] \tag{22}$$

$$m = \frac{dia^*}{dt} \tag{23}$$

$$fc = \frac{Vdc}{HB(8L)}[1 - \frac{4L^2}{Vdc^2}(\frac{Va}{L} + m)^2] \tag{24}$$

This controller is adapted to the proposed system in this paper by Equ.22. According to the equation hysteresis, bandwidth is a function of modulation frequency, supply voltage, dc capacitor voltage and slope of the reference compensator current waveform.
Therefore, the modulation frequency will remain almost constant. This will improve the PWM performances and APF substantially [24].

6. SIMULATION RESULTS

Three-phase voltage source and a nonlinear resistive load connected to the grid via a three-phase diode-bridge rectifier were chosen for the case study and simulation.

International Journal of Mechatronics, Electrical and Computer Technology

Vol. 4(12), Jul, 2014, pp. 857-885, **ISSN**: 2305-0543
Available online at: http://www.aeuso.org

At first the simulation is implemented without the PV-AF. The current which is drawn in harmonic load and one phase of the source is shown in Figure13. The average active and reactive power of the source is also shown in Figure.14. At the following, the PV-AF system is added to the simulated system.The parameters of the system are listed in Table.3. By changing the solar irradiance G=0.75 kw/m^2 and T=23 ^{o}C to G=1kw/m^2 and T=25 ^{o}C at t=0.4s, again by decreasing the irradiance to G=0.5 kw/m^2 and T=18 ^{o}C at t=0.7s the simulation is done.

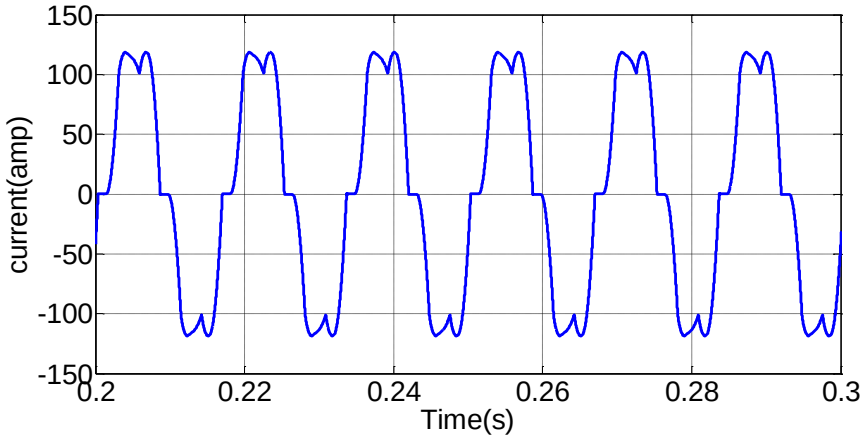

Figure13. Phase current of supply before compensation

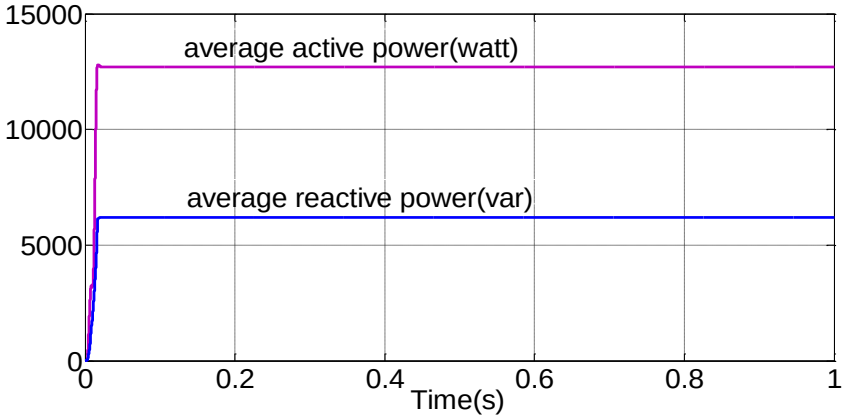

Figure14. Average reactive and active power of one phase

International Journal of Mechatronics, Electrical and Computer Technology

Vol. 4(12), Jul, 2014, pp. 857-885, ISSN: 2305-0543
Available online at: http://www.aeuso.org

Table3: parameter of the simulation

Switching frequency	12KHZ
Fundamental frequency	60 HZ
AC supply voltage	230V
Load resistance	3Ω
Load side inductance	1mH
Inverter side inductor	1mH
Dc link capacitor	1 mF

Figure 15 and Figure 16 shows the changes in solar radiation and temperature. Figure17 shows the generated active power injected by photovoltaic into the grid, and verifies effectiveness of MPPT and injecting of the produced power into the grid using proper reference current. Figure18 and Figure19show the average reactive and active power delivered by supply of one phase and the average reactive and active power delivered by one phase of the PV-AF into the grid. As shown in this figure the active power of the PV decreases the active power generated by supply of the grid; furthermore, this figure shows that the reactive power of the supply is zero; Hence the effectiveness of this proposed method in compensating average reactive power of the load is also verified.The current drawn from the grid and the injected current of the PV-AF are shown in Figure20 and Figure 21 respectively. These figures show that harmonic currents generated by nonlinear loads are compensated by the PV-AP system.

International Journal of Mechatronics, Electrical and Computer Technology

Vol. 4(12), Jul, 2014, pp. 857-885, **ISSN**: 2305-0543
Available online at: http://www.aeuso.org

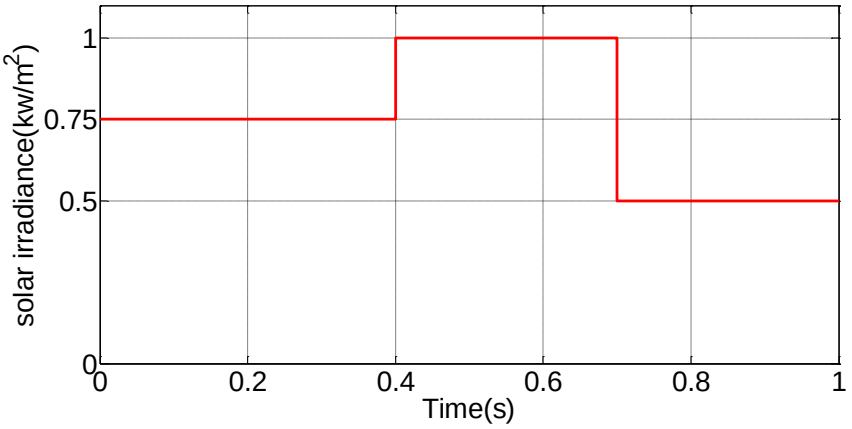

Figure15. Solar radiation

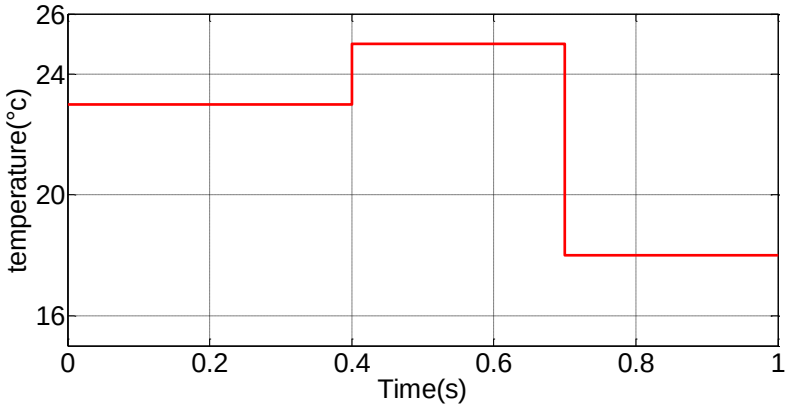

Figure16. Solar temperature

International Journal of Mechatronics, Electrical and Computer Technology

Vol. 4(12), Jul, 2014, pp. 857-885, **ISSN**: 2305-0543
Available online at: http://www.aeuso.org

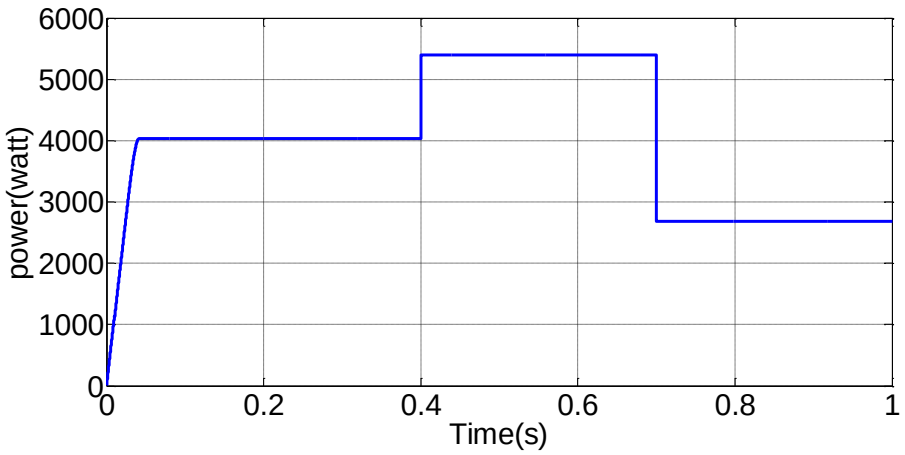

Figure17. Generated active power by the PV

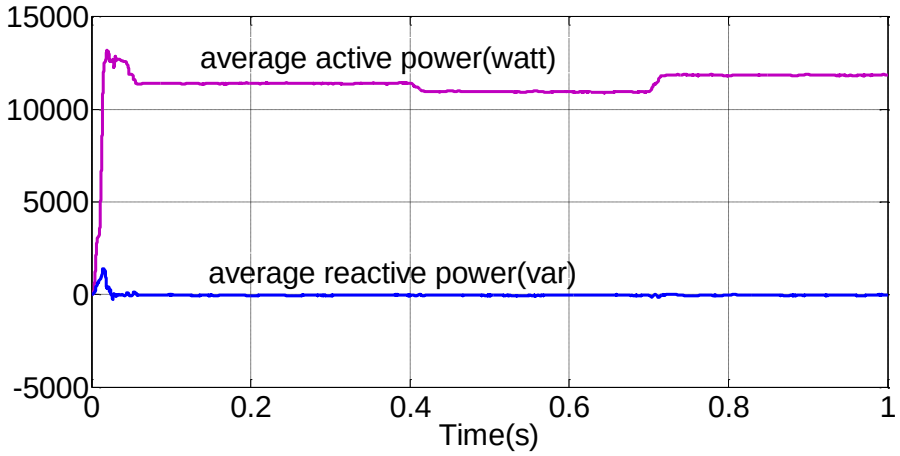

Figure18. Per phase active and reactive power of supply

International Journal of Mechatronics, Electrical and Computer Technology

Vol. 4(12), Jul, 2014, pp. 857-885, **ISSN**: 2305-0543
Available online at: http://www.aeuso.org

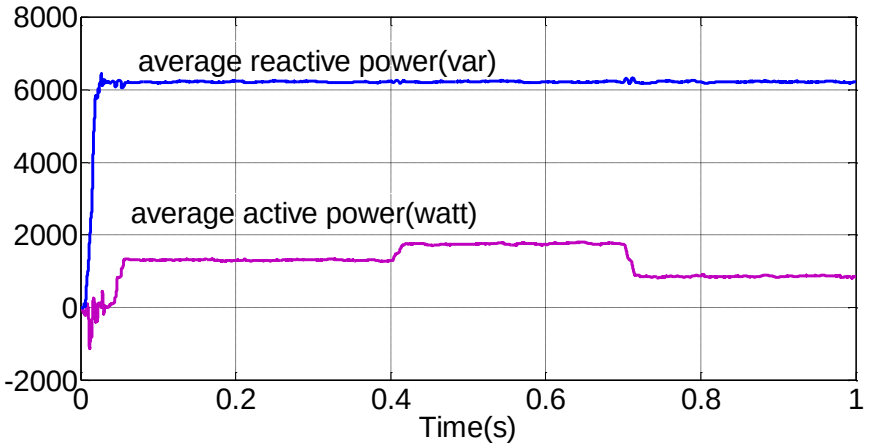

Figure19. Per phase active and reactive power of PV-AF

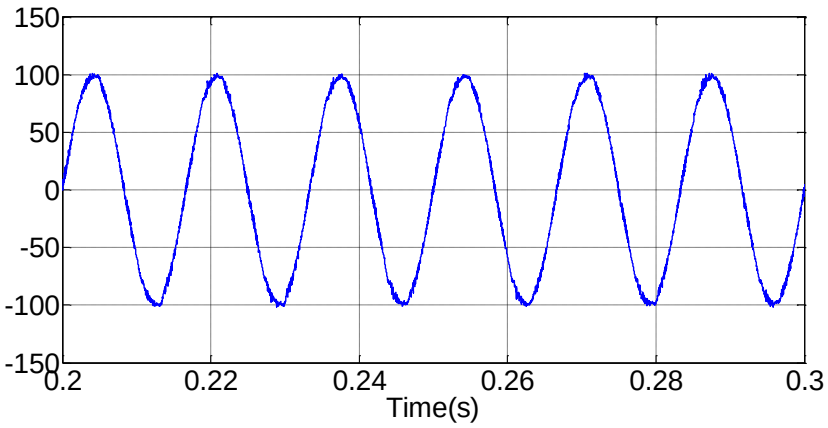

Figure20. Per phase supply current

International Journal of Mechatronics, Electrical and Computer Technology

Vol. 4(12), Jul, 2014, pp. 857-885, **ISSN**: 2305-0543
Available online at: http://www.aeuso.org

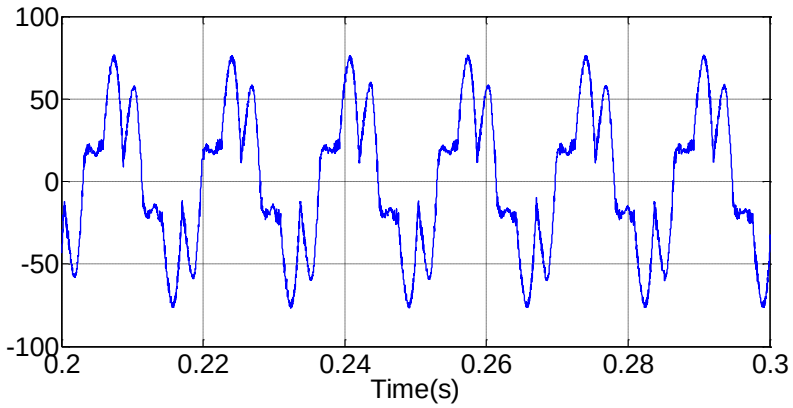

Figure21. Per phase injected current of the PV-AF system

The harmonic spectrum of the supply current before and after compensation is shown in . Figure.22 and Figure.23.The THD (total har-monic distortion) is 18.49% before harmonic compensation in supply current and 1.42%in supply current after harmonic current compensation that is within the limit of the harmonic standard of IEEE 519.

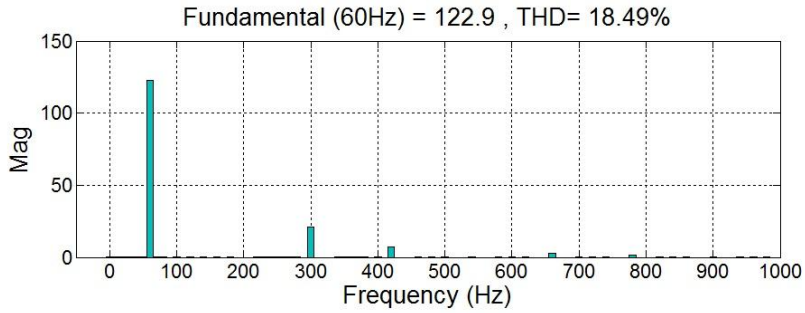

Figure22. Source current's harmonic content without compensation

International Journal of Mechatronics, Electrical and Computer Technology

Vol. 4(12), Jul, 2014, pp. 857-885, **ISSN**: 2305-0543
Available online at: http://www.aeuso.org

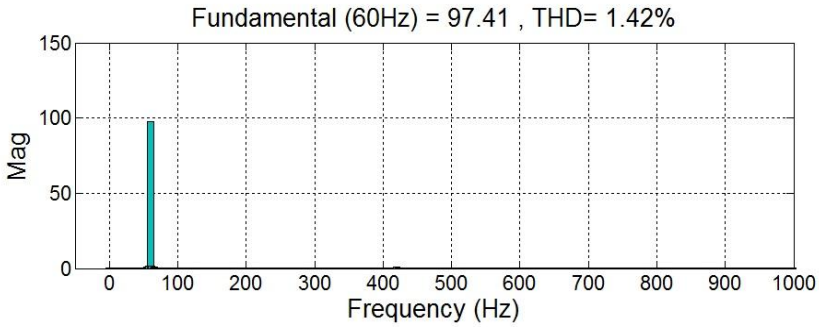

Figure23. Source current's harmonic content with compensation

ThePV- AF is suppressing reactive/harmonic power and simultaneously improves power factor**.** Figure 24and Figure 25 shows the voltage (Vs) and current of the grid (Is) for the phase a. We observe that the current and voltage are in phase because all the reactive power of the load is compensated by the PV system.

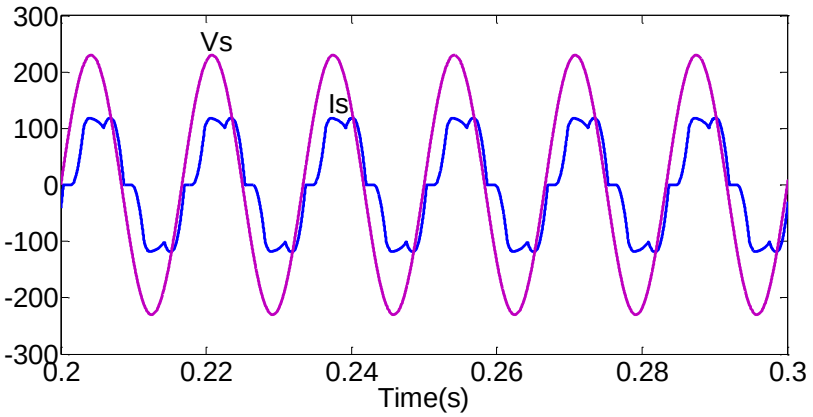

Figure24. Voltage and current of the grid for phase a before compensation.

International Journal of Mechatronics, Electrical and Computer Technology

Vol. 4(12), Jul, 2014, pp. 857-885, **ISSN**: 2305-0543
Available online at: http://www.aeuso.org

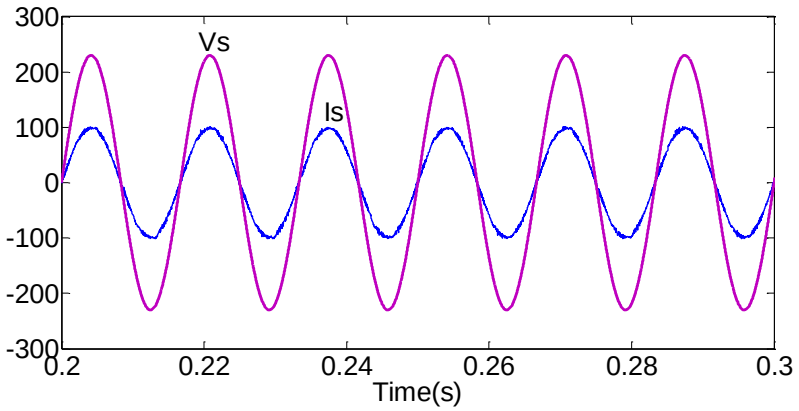

Figure25. Voltage and current of the grid for phase a after compensation.

Conclusion

The main goal of this paper is control of active power and compensates harmonics and reactive power of nonlinear loads and improves the power factor of the power system using PV system. This function of the PV-AF system is done by using proper reference current generation, which is built by the instantaneous power theory (p-q). In this method, the photovoltaic system applies the grid with active power while compensating the reactive power of the load all the day. Simultaneously the PV system is controlled to operate at the maximum power point. Simulation results show that performance of proposed method the PV system is controlled to operate at the maximum power point and the PV-AF can compensate the harmonics and reactive current. Also the THD amount of the current decreases significantly. Using of this configuration is more economical because of replacing separate AF and PV systems by this one for delivering power of PV and filtering simultaneously.

Vol. 4(12), Jul, 2014, pp. 857-885, **ISSN**: 2305-0543
Available online at: http://www.aeuso.org

References

[1] Ersoy Beser, Birol Arifoglu, Sabri Camur, Esra Kandemir Beser "A grid-connected photovoltaic power conversion system with single-phase multilevel inverter," Solar Energy 84 (2010) 2056–2067

[2] R. Belaidi , A. Haddouche , M. Fathi , M. Mghezzi Larafi , A. Chikouche "Improvement of the electrical energy quality using a Shunt Active Filter supplied by a photovoltaic generator," Energy Procedia 6 (2011) 522–530

[3] Exposto, B.; Carneiro, H.; Pinto, G.; Couto, C.; Afonso, J.L "Simulations of a Current-Source Shunt Active Power Filter with Carrier-Based PWM and Periodic ampling Modulation Techniques" Power Electronics and Applications (EPE 2011), Proceedings of the 2011-14th European Conference ,PP.1-8,2011.

[4] A. Messai, A. Mellit, A. Guessoum, S.A. Kalogirou, "Maximum power point tracking using a GA optimized fuzzy logic controller and its FPGA implementation", Solar Energy 85, 265–277, 2011.

[5] Bahgat, A.B.G., Helwa, N.H., Ahmad, G.E., El Shenawy, E.T., "Maximum power point tracking controller for PV system using neural networks", Renewable Energy 30, 1257–1268, 2005.

[6] Chu, C., Chen, C., "Robust maximum power point tracking method for photovoltaic cells", a sliding mode control approach. Solar Energy 83 (8), 1370–1378, 2009.

[7] Mellit, A., Mekki, H., Messai, A., Salhi, H., "FPGA-based implementation of an intelligent simulator for stand-alone photovoltaic system", Expert Systems with pplications 37, 6036–6051, 2010.

[8] Khaehintung, N., Sirisuk, P., "Implementation of maximum power point tracking using fuzzy logic controller for solar-powered lightflasher applications", The 47th IEEE International Midwest symposium on Circuits and Systems, Hiroshima, July 25–28, pp. 171–174, 2004.

[9] B.K. Bose, An adaptive hysteresis band current control technique of a voltage feed PWM inverter for machine drive system, IEEE Trans. Ind Ind. Electron. 37 (5) (1990) 402–406.

[10] Karuppanan P, Kamala Kanta Mahapatra., "PI and fuzzy logic controllers for shunt active power filter — A report", ISA Transactions 51 (2012) 163–169

[11] D B.C Chen; C.L Lin, "Implementation of Maximum-Power-Point Tracker for Photovoltaic Arrays, " Industrial Electronics and Applications (ICIEA), 2011 6th IEEE Conference, P.P.1621-1626,2011.

[12] Weidong Xiao, Magnus G. J. Lind, William G. Dunford, Antoine Capel, "Real-Time Identification of Optimal Operating Points in Photovoltaic Power Systems" , IEEE TRANSACTIONS ON INDUSTRIAL ELECTRONICS, VOL. 53, NO. 4, AUGUST 2006.

[13] Y. Pankow, "Étude de l'intégration de la production décentraliséedansunréseaubasse tension Application aux générateursphotovoltaïques", Thèse de doctorat Centre national de recherché technologique de Lille 2005.

[14] F.Bouchafaa, I.Hamzaoui and A.Hadjammar, "Fuzzy Logic Control for the tracking of maximum power

Vol. 4(12), Jul, 2014, pp. 857-885, **ISSN**: 2305-0543
Available online at: http://www.aeuso.org

point of a PV system", Energy Procedia (Elsevier), vol.6, pp. 633-642, 2011.

[15]BP SX150– 150 watt multi crystalline photovoltaic module datasheet,2001, http://www.southwestpv.com/download.htm

[16] Jen-Cheng Wang1, Yu-LiSu 1, Jyh-CherngShieh,Joe-AirJiang, "High-accuracy maximum power point estimation for photovoltaic arrays", Solar Energy Materials & Solar Cells 95 (2011) 843–851.

[17] Bader N. Alajmi, Khaled H. Ahmed, Stephen J. Finney, Barry W. Williams, "Fuzzy-Logic-Control Approach of a Modified Hill-Climbing Method for Maximum Power Point in Microgrid Standalone Photovoltaic System" , IEEE TRANSACTIONS ON POWER ELECTRONICS, VOL. 26, NO. 4, APRIL 2011.

[18] Chokri Ben Salah, Mohamed Ouali, "Comparison of fuzzy logic and neural network in maximum power point tracker for PV systems", ELSEVIER Electric Power Systems Research 81 (2011) 43–50.

[19] Kalantari, A., et al., A Faster, " Maximum Power Point Tracker Using Peak Current Control", IEEE Symposium on Industrial Electronics and Applications, 2009.

[20] Mei Shan Ngan, Chee Wei Tan, "A Study of Maximum Power Point Tracking Algorithms for Stand-alone Photovoltaic Systems", IEEE applied powet electronics colloquium, 2011.

[21] C. Larbes, S.M. Cheikh, T. Obeidi, A. Zerguerras, "Genetic algorithms optimized fuzzy logic control for the maximum power point tracking in photovoltaic system", Elsevier Ltd, renewable energy 34, pp. 2093- 2100, 2009.

[22] J. Afonso, . Couto and J. Martins , "Active Filters with Control Based on the p-q Theory," IEEE Industrial Electronics Society Newsletter,pp. 5-10, Sept. 2000.

[23] Suresh Mikkili, A.K. Panda, "Real-time implementation of PI and fuzzy logic controllers based shunt active filter control strategies for power quality improvement," Electrical Power and Energy Systems 43 (2012) 1114–1126

[24] We. Dai; Y. Dai; T. Zhong , "A New method for Harmonic and reactive power Compensation" , Industrial Technology, 2008, ICIT 2008. IEEE International Confrence, PP. 1-5, 2008

[25] Satyaranjan Jena, B.Chitti Babu, S.R.Samantaray and Mohamayee Mohapatra, "Comparative Study Between Adaptive Hysteresis and SVPWM Current Control for Grid-connected Inverter System" , 978-1-4244-8942-8/11/$26.00 ©2011 IEEE